Multiple Active Site Conformations Revealed by Distant Site Mutation in Ornithine Decarboxylase[†,‡]

Laurie K. Jackson,[§] Jeffrey Baldwin,[§] Radha Akella,[||] Elizabeth J. Goldsmith,[||] and Margaret A. Phillips*[,§]

Department of Pharmacology and Department of Biochemistry, The University of Texas Southwestern Medical Center at Dallas, 5323 Harry Hines Boulevard, Dallas, Texas 75390-9041

Received May 25, 2004; Revised Manuscript Received August 5, 2004

ABSTRACT: Ornithine decarboxylase (ODC) is an obligate homodimer that catalyzes the pyridoxal 5′-phosphate-dependent decarboxylation of L-ornithine to putrescine, a vital step in polyamine biosynthesis. A previous mutagenic analysis of the ODC dimer interface identified several residues that were distant from the active site yet had a greater impact on catalytic activity than on dimer stability [Myers, D. P., *et al*. (2001) *Biochemistry 40*, 13230−13236]. To better understand the basis of this phenomenon, the structure of the *Trypanosoma brucei* ODC mutant K294A was determined to 2.15 Å resolution in complex with the substrate analogue D-ornithine. This residue is distant from the reactive center (>10 Å from the PLP Schiff base), and its mutation reduced catalytic efficiency by 3 kcal/mol. The X-ray structure demonstrates that the mutation increases the disorder of residues Leu-166−Ala-172 (Lys-169 loop), which normally form interactions with Lys-294 across the dimer interface. In turn, the Lys-169 loop forms interactions with the active site, suggesting that the reduced catalytic efficiency is mediated by the decreased stability of this loop. The extent of disorder varies in the four Lys-169 loops in the asymmetric unit, suggesting that the mutation has led to an increase in the population of inactive conformations. The structure also reveals that the mutation has affected the nature of the ligand-bound species. Each of the four active sites contains unusual ligands. The electron density suggests one active site contains a gem-diamine intermediate with D-ornithine; the second has density consistent with a tetrahedral adduct with glycine, and the remaining two contain tetrahedral adducts of PLP, Lys-69, and water (or hydroxide). These data also suggest that the structure is less constrained in the mutant enzyme. The observation of a gem-diamine intermediate provides insight into the conformational changes that occur during the ODC catalytic cycle.

Ornithine decarboxylase (ODC)[1] catalyzes the decarboxylation of L-ornithine (L-Orn) to the diamine putrescine (Put), a crucial step in polyamine biosynthesis (*1*−*4*). Cells that are depleted of polyamines undergo growth arrest and do not progress through the cell cycle. Because of the importance of polyamines to cell growth, ODC has been investigated as a therapeutic target for a number of proliferative diseases. Most notably, ODC has proven to be an effective target in the treatment of African sleeping sickness, a fatal tropical disease.

ODC is a pyridoxal 5′-phosphate (PLP)-dependent enzyme that is a member of the fold type III PLP family, which includes alanine racemase (*5*−*8*). These enzymes are obligate homodimers, and the active site is formed at the dimer interface between the N-terminal β/α-barrel domain of one subunit and the C-terminal, β-barrel domain of the second subunit (Figure 1). The N-terminal domain contains an active site Lys residue (Lys-69) that binds PLP through a Schiff base (internal aldimine). Substrate binding displaces this interaction through a series of steps that include the formation of (1) a noncovalent Michaelis complex, (2) a tetrahedral gem-diamine intermediate, and (3) the Schiff base (external aldimine) between L-Orn and PLP. Once L-Orn is bound as a Schiff base, the conjugated π system of PLP facilitates decarboxylation (*9*). Decarboxylation is followed by protonation and product release, which is rate-limiting, regenerating the internal aldimine (*10*). Previous structural analysis has provided evidence for the Schiff base species between PLP and Lys-69 [uncomplexed native enzyme (*8*)] and for the Schiff base species with the product putrescine and with substrate analogues [D-Orn and DFMO (*11*, *12*)].

ODC buries a significant amount of surface area (2775 Å^2) along the dimer interface (*8*). Ala-scanning mutagenesis of residues in the *Trypanosoma brucei* ODC dimer interface suggested that the energetic contribution of these residues to dimerization was distributed across the interface such that mutation of any single residue had little impact on dimerization (*13*). In contrast, the analysis demonstrated that a number of dimer interface residues are instead important for ODC activity, and this finding extended to a subset of

[†] This work was supported by grants from the National Institutes of Health (R01 AI34432 to M.A.P.) and the Welch Foundation (Grant I-1257 to M.A.P. and Grant I1128 to E.J.G.). M.A.P. is a recipient of a Burroughs Welcome Fund Scholar Award in Molecular Parasitology.

[‡] The coordinates have been deposited as entry 1SZR.

* To whom all correspondence should be addressed. Telephone: (214) 648-3637. Fax: (214) 648-9961. E-mail: margaret.phillips@UTSouthwestern.edu.

[§] Department of Pharmacology.

[||] Department of Biochemistry.

[1] Abbreviations: ODC, ornithine decarboxylase; L-Orn, L-ornithine; D-Orn, D-ornithine; PLP, pyridoxal 5′-phosphate; DFMO, α-difluoromethylornithine; Put, putrescine; K294A ODC, ODC with Lys-294 mutated to Ala.

10.1021/bi048933l CCC: $27.50
Published on Web 09/23/2004

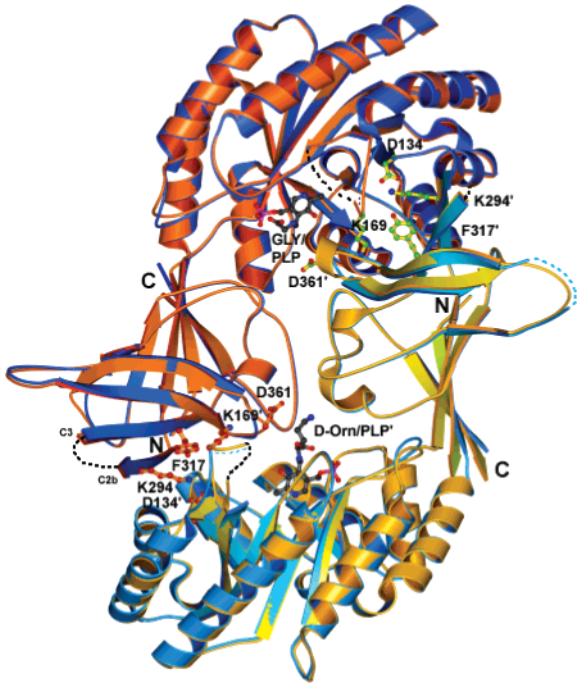

FIGURE 1: Ribbon diagram of *T. brucei* K294A ODC superimposed with coordinates from wild-type *T. brucei* ODC complexed with putrescine (ODC/Put) (PDB entry 1f3t) (*11*). This figure was drawn with Molscript (*39*) and rendered with PovRay (*40*). Individual monomers of K294A ODC are colored navy or light blue. Individual ODC/Put monomers are colored orange or gold. PLP/D-Orn (active site B) or PLP/Gly (active site A) from K294A ODC is rendered as a ball-and-stick diagram with carbon atoms rendered as black balls, and all atoms are connected with black sticks. Selected residues, including Lys-294, from ODC/Put are displayed, and labeled with a prime to distinguish between the subunits. Carbon atoms from the ODC/Put structure are rendered with either orange or green balls connected by orange or yellow sticks. All nitrogen atoms are colored blue, oxygens red, and phosphorus atoms pink.

residues that were distant from the active site. Thus, the dimer interface of ODC is optimized to promote catalysis and not to maximize the protein−protein interaction.

One of the largest effects on catalytic activity caused by the mutation of a distant site, dimer interface residue occurred at Lys-294, located more than 10 Å from the active site cofactor and ligands (*13*). Lys-294 is located within the β-sheet domain where it forms hydrogen bond and salt bridge interactions across the dimer interface with residues from the β/α-barrel domain of the opposite monomer (Figure 1). Approximately 90 Å^2 of solvent-accessible surface area from this residue is buried upon ODC dimerization (*13*). Interestingly, while this residue is conserved in the most closely related homologues to *T. brucei* ODC (e.g., mammalian and frog), it is not an invariant residue, suggesting that its function is linked to sequence context.

To understand the structural basis for the mutational effects on ODC activity from this long-range interaction, we have determined the X-ray structure of K294A ODC bound to the substrate analogue D-ornithine (D-Orn) to 2.15 Å resolution. The loop from Leu-166 to Ala-172 (Lys-169 loop), which forms hydrogen bonding interactions with Lys-294 in wild-type ODC, is destabilized and becomes more disordered. This primary feature apparently renders the active site more permissive, as up to three different complexes are observed at the four different active sites in these crystals. The most interesting is the tetrahedral gem-diamine of PLP with D-Orn and Lys-69, which has not previously been observed. Model building suggests that, due to steric constraints upon binding, the gem-diamine with L-Orn substrate will be analogous to the diamine with D-Orn, and thus, the structure reveals how the bond between the substrate αN group and the C4′ atom of PLP starts perpendicular to the plane of the PLP before rotating to form a planar system with PLP. Comparisons with the structure of native ODC with an internal aldimine (*8*) and ODC in complex with the product Put (ODC/Put) (*11*) reveal further conformational changes that take place during the catalytic cycle.

EXPERIMENTAL PROCEDURES

Materials

Polyethylene glycol was obtained from Hampton, and all other chemicals were purchased from Sigma.

Methods

ODC Expression and Purification. The creation of the K294A *T. brucei* ODC mutant was described previously (*13*). The mutant protein was purified as described for wild-type ODC (*8*, *11*, *14*). For crystallization, the His tag was removed by TEV protease digestion as described previously (*15*).

Steady-State Assays of ODC Activity. The steady-state rates were measured over a range of enzyme and substrate concentrations at 37 °C, in the presence of excess free PLP (0.2 mM) using a previously described (*14*) enzyme-linked spectrophotometric assay that is based on the CO_2 detection kit (Sigma Diagnostics, St. Louis, MO). Enzyme and substrate levels were as follows: for K294A ODC, [E] = 50−400 nM and [S] = 3−87.5 mM, and for wild-type ODC, [E] 10−40 nM and [L-Orn] = 0.2−6 mM. To determine an apparent binding affinity for PLP, the concentration of free PLP (0−0.16 mM) was varied at a fixed L-Orn concentration (50 mM) and the activity of the mutant (200 nM) or wild-type ODC (50 nM) measured. The concentration dependencies of the decarboxylation rates were fitted to eq 1

$$v = \frac{V_{max}[L]}{K_m + [L]} \quad (1)$$

with Sigma Plot 2001 version 7.0 (SPSS Inc., Chicago, IL), where the *y* intercept (*b*) was set to equal background rates (0.002 OD/min), to determine the kinetic constants. The analytical ultracentrifugation conditions used to assess dimerization of wild-type and mutant ODC enzymes [100 mM Hepes (pH 7.5), 100 mM NaCl, 0.5 mM 2-mercaptoethanol, and 0.02 mM PLP at 20 °C (*13*)] differ from those in the steady-state decarboxylation assay (buffer pH 8, 9 mM magnesium, 2 mM DTT, 0.2 mM PLP, 2 mM phosphoenolpyruvate, 200 mM glycerol, and L-Orn at 37 °C).

Crystallization. T. brucei K294A ODC was crystallized under the following conditions. Equal volumes of *T. brucei* K294A ODC [20 mg/mL in 10 mM Hepes (pH 7.2), 50 mM NaCl, 10 mM DTT, 0.5 mM EDTA, 0.01% Brij-20, and 40 mM D-Orn] and well solution [18% polyethylene glycol 3350, 100 mM Hepes (pH 7.0), 200 mM NH_4OAc, 100 mM glycine, and 10 mM DTT] were mixed to form sitting drops (vapor diffusion method). Crystals formed in 1−3 days at 16 °C. Crystals were cryoprotected in 1.2×

Table 1: Data Collection, Processing, and Refinement Statistics for the Determination of the *T. brucei* K294A ODC Structure

Data Collection and Processing	
wavelength (Å)	1.03320
resolution (Å)	2.15
total no. of reflections	1659505
no. of unique reflections	84756
completeness (%) (last shell $I > \sigma$)	94.5 (96.1)
redundancy	19.6
intensities I/σ (last shell)	21.1 (2.4)
χ^2	1.118
R_{merge}	0.074
Refinement	
no. of reflections ($F > 2\sigma$)	68038 (35−2.15)
no. of non-H protein atoms	11057
no. of water molecules	260
R_{cryst} (%)/R_{free} (%) ($F > 2\sigma$)	24.4/ 27.9 (35−2.15)
rmsd for bond lengths (Å)	0.0078
rmsd for bond angles (deg)	1.238
average *B*-value (Å^2)	42
B rmsd for bonded main chain atoms	0.561
B rmsd for bonded side chain atoms	0.854

crystal conditions with 20% polyethylene glycol 400 and then frozen in propane.

Data Collection and Processing. Diffraction data were collected at beamline 19-ID (SBC-CAT) at the Advanced Photon Source (Argonne National Laboratory, Argonne, IL). Data were indexed, integrated, and scaled using the HKL2000 program package (*16*). Data processing statistics are summarized in Table 1.

Structure Determination and Refinement. The coordinates of a dimer from the *T. brucei* K69A ODC structure complexed with DFMO (*8*) (PDB entry 2tod), with DFMO, waters, and the side chains for Lys-294 and Cys-360 removed, were used as a search model to calculate initial phases by molecular replacement using AMoRe (*17*). The model for K294A ODC was built in O version 6.2.2 (*18*) and refined utilizing data collected between 35 and 2.15 Å until an R_{free} of 32 was reached using CNS (*19*). Additional rounds of refinement were conducted using Refmac 5 (CCP4) (*20*, *21*) to take advantage of the use of TLS parameters (*22*). An identical set of test flags was maintained in reflection files between CNS and CCP4 programs. Water molecules were added using both CNS and Refmac5 and edited in O. Medium noncrystallographic symmetry constraints were kept for initial rounds of refinement, and released for several rounds, and then restraints were added again for the remainder of the refinement. PROCHECK (*23*) confirmed that no peptide torsion angles in our K294A ODC model were found in disallowed regions of a Ramachandran plot, while 1086 of 1198 non-glycine and non-proline residues fall within the most favored regions. Final refinement statistics were calculated in CNS and are listed in Table 1.

Determination of the Overall Root-Mean-Square Deviation. Coordinates from the structures of K294A ODC, ODC complexed with putrescine (ODC/Put) (PDB entry 1f3t) (*11*), or K69A ODC complexed with DFMO (K69A ODC/DFMO) (*8*) (PDB entry 2tod) were edited to include only shared amino acid residues 37−157, 171−296, 312−340, and 350−408, and then they were superimposed as either monomers or dimers in InsightII (Accelrys). The rms deviation for each residue was obtained in CNS. The main chain rmsd was calculated by averaging over all residues.

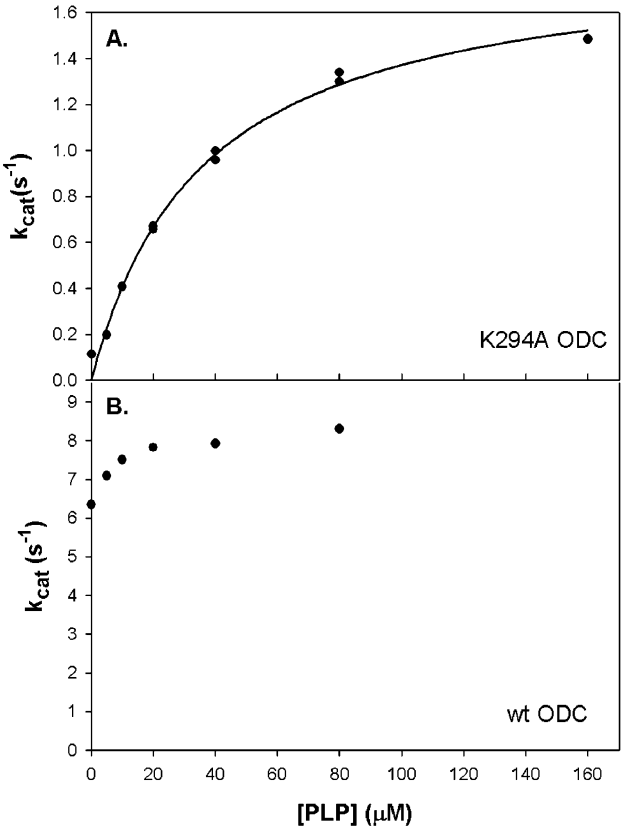

FIGURE 2: Dependence of ODC activity on PLP concentration. Plots showing enzyme activity at 50 mM L-Orn for either (A) K294A ODC (200 nM) or (B) wild-type ODC (50 nM) over a range of PLP concentrations. Plots were created using SigmaPlot 2001 (SPSS Inc.). Data are shown as filled circles. The K294A ODC data have been fit to eq 1, and the fit is rendered as a solid line.

Collection of UV−Vis Spectra for Wild-Type and K294A ODC with and without Putrescine or D-Orn. UV−vis spectra (250−500 nm) for wild-type (60 μM) and K294A ODC (200 μM) were collected in Hepes (150 mM, pH 8) at room temperature with or without putrescine or D-Orn (50 mM, pH 8). Enzyme was first desalted into fresh buffer to eliminate any excess free PLP. After spectral scans had been taken, K294A ODC (with or without putrescine) was centrifuged using a Centricon YM-10 ultrafiltration device (MW cutoff of 10 000) (Millipore Corp., Bedford, MA), and the flow through (less than half of the starting volume) was analyzed spectrally to assess PLP dissociation. Less than 2% of the PLP dissociated from unliganded K294A ODC and less than 20% in the presence of putrescine.

RESULTS

Steady-State Analysis of K294A ODC Activity. The effect of free PLP on ODC activity was determined under steady-state conditions using 50 mM L-Orn and either K294A ODC (200 nM) or wild-type ODC (50 nM). While nearly maximal activity is observed for wild-type ODC in the absence of free PLP, a clear titration of K294A ODC activity is observed as the concentration of free PLP is increased (Figure 2). A fit of these data yielded an apparent K_m for PLP of 36 μM for K294A ODC, a 240-fold increase over the K_m for PLP in the wild-type enzyme (previously reported to be 0.15 μM) (*24*). The value for K294A ODC is similar to that observed for R277A mutant ODC; this residue forms a salt bridge

Table 2: Steady-State Kinetic Analysis of K294A and Wild-Type ODC[a]

ODC protein	K_m(L-Orn) (mM)	k_{cat} (s^{-1})	k_{cat}/K_m(L-Orn)	K_m(PLP) (μM)
K294A	43 ± 5	3.5 ± 0.3	0.08	36 ± 3[b]
wild type	0.37 ± 0.04	15.4 ± 0.2	41.6	0.15[c]

[a] All reported errors are standard deviations of the mean ($n = 3$). [b] Standard error of the fit. [c] Data taken from ref *24*. k_{cat}/K_m is in units of mM^{-1} s^{-1}.

with the phosphate moiety of PLP (*24*). These data suggest that the affinity for PLP has been altered in this mutant.

The steady-state kinetic parameters k_{cat} and K_m (for L-Orn) were determined for both wild-type (20−40 nM) and K294A ODC (150−300 nM) in the presence of 200 μM free PLP, which is saturating for both enzymes (Table 2). The k_{cat} measured for K294A ODC (3.5 s^{-1}) is 4-fold lower and the value for K_m (43 mM) 114-fold higher than the corresponding parameters for wild-type ODC. Values of k_{cat} and K_m for K294A and wild-type ODC have been reported previously but under conditions where free PLP was limiting [50 μM (*13*)].

At lower enzyme concentrations (50−150 nM), the k_{cat} for K294A ODC had a small but reproducible dependence on enzyme concentration (data not shown), suggesting that the dimer may not be fully stable under the assay conditions. However, the effect was not sufficiently significant to utilize the kinetic analysis to derive a K_d for dimerization. Steady-state kinetic data were thus collected at enzyme concentrations above 150 nM to ensure full dimer formation under assay conditions. For the wild-type enzyme, no enzyme concentration dependence on k_{cat} is observed above 20 nM. Previous analysis of dimer formation for K294A ODC by analytical ultracentrifugation suggested that the K_d for dimer formation was not significantly affected (*13*). Differences in salt and temperature conditions may account for the observed disparity in dimerization between these two experimental methods.

Crystallization, Data Collection, and Structure Determination. The molecular structure of *T. brucei* K294A ODC was determined using space group $P2_12_12_1$ ($a = 67.5$ Å, $b = 152.4$ Å, and $c = 155.0$ Å) to 2.15 Å resolution. The final model contains four monomers in the asymmetric unit (which are labeled A−D), in the form of two homodimers, containing a total of 1414 amino acid residues, four PLP molecules, and 260 water molecules. Chains A and B form the first dimer in the asymmetric unit, and chains C and D compose the second. The *R*-factor is 24.4% with an R_{free} of 27.9% for data between 35 and 2.15 Å (Table 1). These *R*-factors are similar to those observed for previous *T. brucei* ODC structures, and the relatively high R_{free} is probably due to the high percentage of disorder (20%) and unmodeled differences between the subunits, especially in these disordered regions. The refinement yielded interpretable density (minimally) for amino acid residues 37−157, 169−296, and 312−408 for all monomers, with the exceptions that density for residues 345−348 of monomer B could not be interpreted. Additionally, while weak density for residues 169 and 170 for monomer A was observed, positions and orientations for these residues could not be determined unambiguously, so they were omitted from the final coordinates. Monomer D had additional definable density at the N-terminus, for residues 14−30, and monomer B had additional density for residues 409−420 at the C-terminus.

Different Adducts Occupy the Four Active Sites. The electron density in the active sites of the K294A ODC structure suggests that they are differentially occupied with D-Orn, glycine, or water. The active site at the interface between the β/α-barrel of monomer B and the β-sheet domain of monomer A (defined as active site B) contains density that unambiguously can be assigned to a complex with a D-Orn molecule, bound in a gem-diamine to PLP, with Lys-69. This active site will be discussed in greater detail below and will be the active site region used in structural comparisons throughout this paper. Within the same dimer, active site A shows density that is consistent with a molecule of glycine (used as an additive in the crystal conditions), bound in a tetrahedral adduct with Lys-69 and PLP (gem-diamine). Strong density is observed for the αN, Cα, and COO moieties of Gly, while no density is observed that would indicate the presence of a side chain in this active site. Attempts made to refine the structure with a D-Orn in the A active site resulted in the appearance of negative density in a $2F_o - F_c$ map. Thus, the ligand was modeled as a Gly. However, we cannot rule out the possibility that this active site contains D-Orn, and that density for the side chain is missing due to partial disorder or multiple occupancy. Active sites in the second dimer, C and D possess no large adducts to PLP. However, positive density in the $F_o - F_c$ map observed at the C4′ position of PLP, opposite from Lys-69 (data not shown), suggests that PLP exists as a carbinolamine (the tetrahedral adduct that includes Lys-69 and hydroxide). PLP-tetrahedral carbinolamine has been observed spectrally in solution at high pH (*25*).

D-Orn Gem-Diamine, Active Site B. In active site B, D-Orn is bound as a tetrahedral adduct among Lys-69, PLP, and D-Orn (Figures 3 and 4). The D-Orn is near the surface of ODC on the opposite side of the PLP with respect to Lys-69. Significant conformational differences are present between the gem-diamine and the external aldimine. In the gem-diamine structure, the αN group of D-Orn forms a H-bond with the side chain of His-197 (3.3 Å from Nϵ2 of His-197). In the external aldimine (such as with ODC/Put), the αN atom of the substrate is in the plane of the PLP, forming interactions with the phenolic oxygen of PLP, which positions it away from His-197 (Figures 4 and 5) (*11*). In the external aldimine structure, the positioning of these groups leads to the formation of a conjugated π system more planar than that observed for the gem-diamine.

There are other conformational differences local to the gem-diamine as well. Cys-360, which has been observed in two different conformations in various ODC structures, is observed in multiple conformations in this structure. In the active site that contains D-Orn (B) and in active site C, it is positioned in the "down" conformation pointing away from D-Orn. This is the conformation observed previously in native ODC (*8*) and in an inhibited ODC complex with D-Orn (ODC/D-Orn/G418) (*12*). In active sites A and D, Cys-360 is in the "up" conformation pointing toward the PLP, which is the position previously observed for the product complex structures (*8*, *11*). Density for Cys-360 residues modeled in the up orientation was weak, and it is possible that these Cys-360 residues exist in more than one orientation, and that the observed density is an average of this partial occupancy.

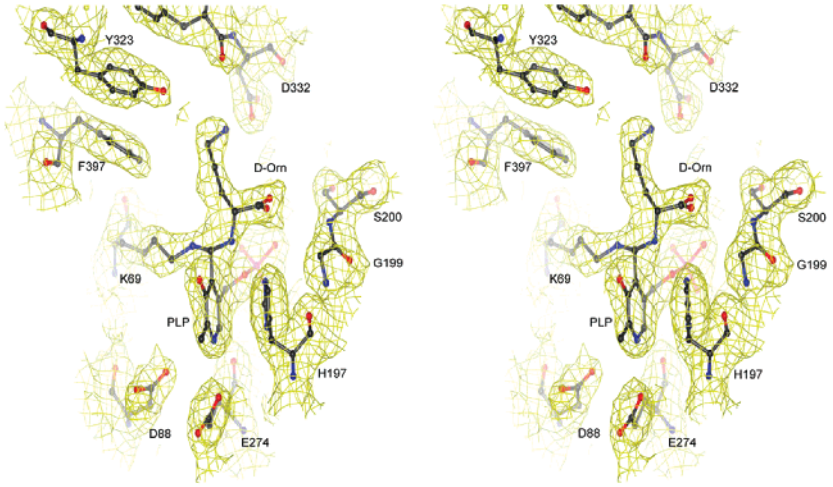

FIGURE 3: Electron density map (stereoview) for the K294A ODC active site. Active site B is displayed showing that a stable tetrahedral binding intermediate (gem-diamine) has formed among Lys-69, PLP, and D-Orn. The weighted difference maps, generated by Refmac5 (*41*), are rendered in yellow, contoured at 1.0σ with Bobscript (*40*, *42*) using a gl render interface (L. Esser, personal communication). The PLP cofactor, D-Orn ligand, and amino acid residues are rendered as balls and sticks with carbon atoms colored black, oxygens red, and nitrogens blue.

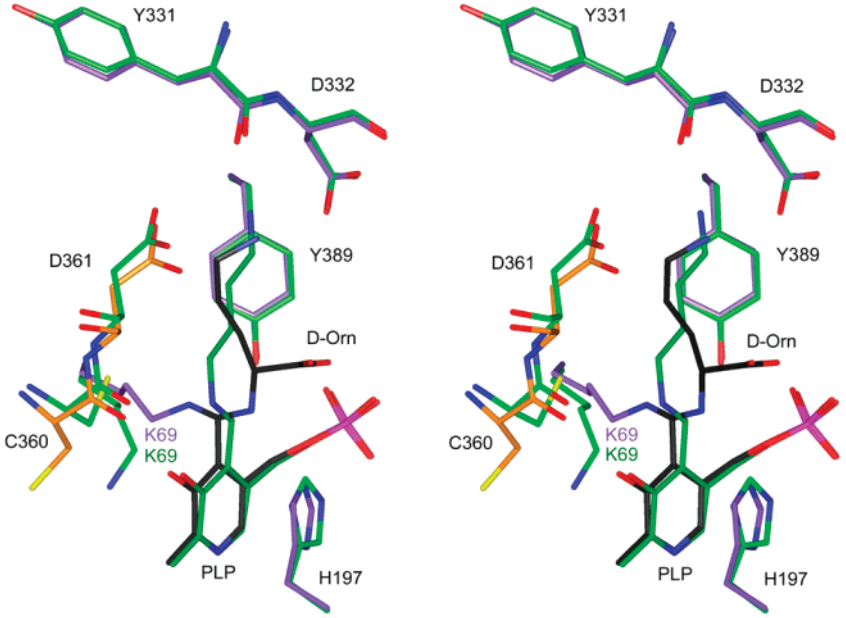

FIGURE 4: Comparison of the K294A ODC active site with wild-type ODC complexed with putrescine. The active site residues, cofactor, and ligands are displayed for the K294A ODC and ODC/Put structures (*11*) using InsightII. Coordinates were superimposed via backbone atoms of selected active site residues (B274, B277, B331, and B389). For the K294A ODC structure, carbon atoms of monomers A and B are colored differently. Carbon atoms are colored orange for K294A ODC monomer A and purple for monomer B. PLP and D-Orn carbon atoms are colored black. All carbon atoms from the ODC/Put structure are colored green. All nitrogen atoms are colored blue, oxygens red, sulfurs yellow, and phosphorus atoms pink.

Ala-294 Site at the Dimer Interface. The K294A mutation induces increased disorder in a loop forming the subunit interface and active site. In native ODC, Lys-294, which belongs to strand C2b (Figure 1), bridges the homodimer (Figure 6) by binding to two loops in the β/α-barrel from the opposite monomer, the Lys-169 loop, and a loop containing Asp-134. The Lys-169 loop is a locus of disorder in the various *T. brucei* ODC structures that have been determined. Nϵ of the Lys-294 side chain forms hydrogen bonds to the backbone carbonyl oxygen of Lys-169 and the side chain oxygens (γO) of Asp-134 from the opposite monomer. Asp-134 in turn forms hydrogen bond interactions with Phe-170, further stabilizing the Lys-169 loop. The position of these residues is mainly unaltered in the Ala-294 structure. However, the loop containing Lys-169 becomes more disordered in the mutant. Residues Val-158−Arg-165 are disordered in all five *T. brucei* ODC structures that have been determined (Table 3), but in the mutant, Leu-166 and Ser-167 are also disordered in all four monomers. Disorder of Leu-166 and Ser-167 was also previously observed in the ODC/D-Orn/G418 structure (*12*). Finally, the disorder observed near active site A is more extensive than in the other monomers; the locus of the Gly adduct, Val-168, Lys-169, and Phe-170 are also in weak density, suggesting that the mutation has relaxed the protein, allowing it to more readily adapt multiple conformations. The absence of the Lys-294 side chain H-bond with the backbone carbonyl of Lys-169 is likely a contributing factor in this disorder.

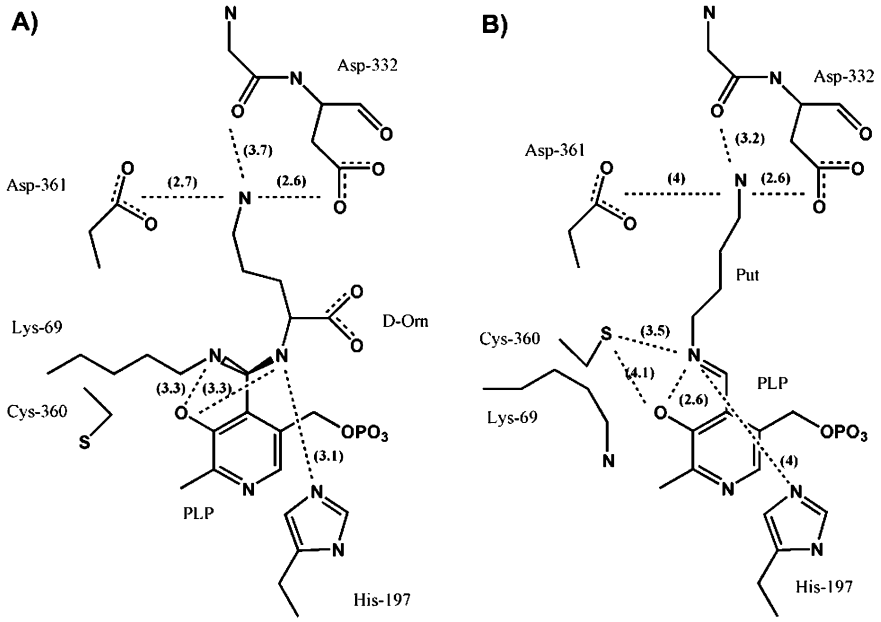

FIGURE 5: Two-dimensional diagram of the ODC active site. (A) K294A ODC active site containing the tetrahedral complex of Lys-69, PLP, and D-Orn and (B) wild-type ODC active site complexed with putrescine. Distances between the PLP cofactor, ligand, and selected active site residues are shown. The figure is not drawn to scale. Backbone atoms only are drawn for Tyr-331. Lys-69 is drawn to the side for clarity. Sketches were drawn with Chemdraw Ultra (CambridgeSoft Corp., Cambridge, MA).

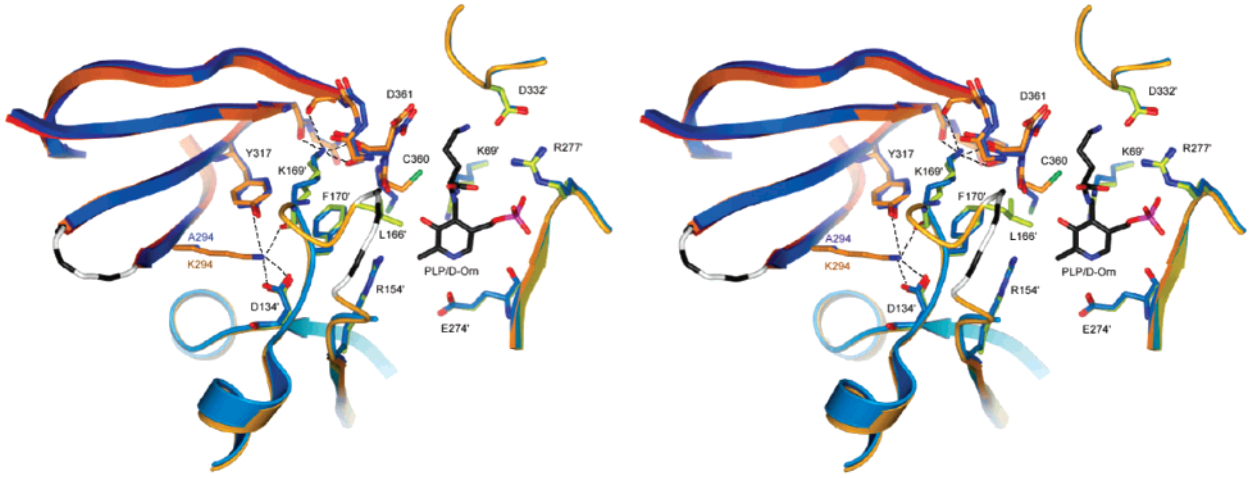

FIGURE 6: Residues in the pathway between Lys-294 and the ODC active site. Selected residues from K294A ODC are displayed (stereoview), superimposed with corresponding residues from the ODC/Put X-ray crystal structure (PDB entry 1f3t) (*11*). Coordinates were superimposed via backbone atoms of selected active site residues (B274, B277, B331, and B389), drawn with Molscript (*39*), and rendered with PovRay (*40*). For the K294A ODC structure, secondary structure and carbon atoms are colored light blue or navy blue. For the ODC/Put structure, secondary structure and carbon atoms are colored orange or yellow. PLP and D-Orn carbon atoms are colored black. PLP and ligand are displayed from the K294A ODC structure only. All nitrogen atoms are colored blue, oxygens red, sulfurs yellow, and phosphorus atoms pink. Residues that may form hydrogen bond interactions with Lys-294 and Lys-169 are connected to the respective Lys with a dashed line. Black and white coil denote disordered regions and are drawn to connect ordered residues of ODC/Put.

The disorder in the Lys-169 loop is likely to explain the structural basis for the reduced catalytic activity of the mutant enzyme. Residues that become disordered in the loop either are involved directly in the active site or form interactions with important catalytic residues. First, on the basis of its position in the ODC/Put structure, Leu-166 is within 4.5 Å of the carboxylate of D-Orn in the K294A ODC gem-diamine structure. Modeling suggests that it will also be near the carboxylate of L-Orn in the gem-diamine, but not the Schiff base structure, and thus, it could potentially be involved in direct interactions with the substrate during the catalytic cycle. Second, other residues in the loop have second-shell interactions with the active site. Lys-169 forms hydrogen bonding interactions across the dimer interface with four residues [Gly-357 (3 Å), Thr-359 (2.5 Å), Asp-361 (3.2 Å), and Asp-364 (3.3 Å)] in the "catalytic loop", and Phe-170 (3.3 Å) is within van der Waals distance of the carbonyl of Cys-360 (Figure 6). Asp-361 interacts directly with ligand (Figures 4 and 5), and is essential for substrate binding, while evidence suggests that Cys-360 is a catalytic base (*11*, *26*). Interestingly, the effects of mutation of either Lys-169 or Phe-170 to Ala on the catalytic efficiency of the enzyme are similar to that for the K294A mutant [k_{cat}/K_m is reduced by 3−4 kcal/mol (*13*)].

Structural Comparison between K294A and Wild-Type ODC and Other ODC Complexes. Outside of the increased disorder of the Lys-169-loop, conformational differences between K294A ODC and wild-type ODC are small and

Table 3[a]

structure	chain (monomer)	disordered residues	disordered residues
K294A ODC	A	158−170	297−311
K294A ODC	B	158−168	298−310
K294A ODC	C	158−167	297−311
K294A ODC	D	158−167	297−311
ODC/Put	A	158−167	297−311
ODC/Put	B	159−165	297−311
ODC/Put	C	160−164	297−311
ODC/Put	D	158−165	297−311
ODC/D-Orn/G418	A	158−167	297−311
ODC/D-Orn/G418	B	158−167	297−311
ODC/D-Orn/G418	C	158−167	297−311
ODC/D-Orn/G418	D	158−167	297−308
native ODC	A−D	158−165	297−310
K69A ODC/DFMO	A−D	158−165	298−310

[a] Amino acid residues from two internal regions that are found to be disordered in *T. brucei* ODC structures are listed for each chain. K294A ODC refers to the structure reported in this paper, ODC/Put the structure of wild-type ODC in complex with ODC's reaction product putrescine (*11*), and ODC/D-Orn/G418 the structure of wild-type ODC in complex with D-Orn and G418 (*12*). Native ODC is the wild-type, unliganded ODC (*8*), and K69A ODC/DFMO refers to the structure of a K69A mutant ODC that has been irreversibly inactivated with difluoromethylornithine (DFMO) (*8*).

distributed throughout the protein. The rmsds were below 0.25 Å for superposition of individual domains, below 0.3 for superposition of monomers (K294A vs wild-type ODC/Put), and below 0.43 Å for superposition of dimers. The differences in these numbers are due to slight domain and subunit rotations. Similar results were obtained when K294A ODC was superimposed with K69A ODC/DFMO. To determine where the largest conformational changes occurred relative to the mutation, we analyzed the conformational change within a single subunit by superimposing the C-terminal domains of K294A ODC with the wild-type native ODC structure (PDB entry 1QU4, superimposed). In this alignment, the N-terminal domains show the greatest rmsd, a reflection of a slight domain rotation between the structures (Figure 7). Some discrete sites also show greater variation. These spikes largely occur at sites of conformational changes observed previously in ODC and in surface loops. Conformational differences were observed at similar loci between ODC/Put and native ODC (empty), with a correlation coefficient of 0.3 for changes within individual domains (correlation coefficient calculated as the average value of the cosine of the angle between the shift vectors for Cα atoms of K294A ODC − native ODC vs ODC/Put − native ODC).

Comparison of UV−Vis Spectra for K294A and Wild-Type ODC with or without the Product. The spectral properties of the PLP cofactor provide insight into the electronic and tautomeric states of the cofactor (*27*). To assess the state of ligation of K294A in solution, UV−vis spectra were measured for product (Put) complexes of K294A and wild-type ODC (Figure 8). Both the native and putrescine-complexed, wild-type enzyme exhibit comparable spectra, with 340 nm absorption maxima and a significant 420 nm peak due to the internal and external aldimine. Unliganded K294A ODC has similar spectra. The spectrum of putrescine-bound K294A is very different, with a larger maximum at 415 nm and almost no peak at 335 nm. Similar spectra were obtained with and without D-Orn (data not shown). Subtracting the flow-through spectra after ultrafilitration from the

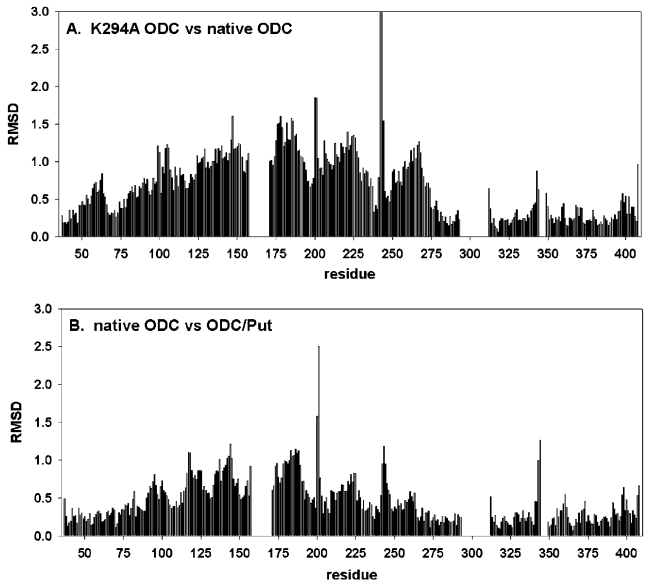

FIGURE 7: Root-mean-square deviation (rmsd) vs residue number for (A) K294A ODC chain A and native ODC or (B) native ODC vs ODC/Put, where the C-terminal domains (residues 37−43 and 281−408) have been superimposed in InsightII.

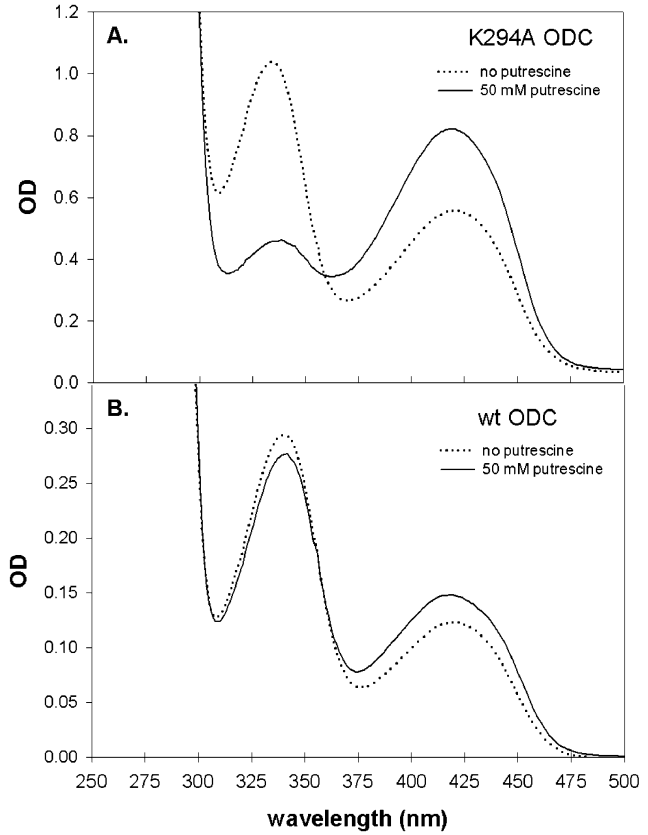

FIGURE 8: Spectra (from 250 to 500 nm) obtained from either 200 μM K294A ODC (A) or 60 μM wild-type ODC (B), either with (—) or without (•••) 50 mM putrescine.

K294A ODC spectra does not significantly affect the size of the observed change, indicating that the dramatic shift in the maximum is not due to PLP dissociation. These results provide additional evidence that the K294A mutation alters the liganded active site structure. However, the spectrum with a large maximum at 420 nm is still characteristic of an sp^2 hybridized (C4′) Schiff base species. In contrast, a gem-

diamine exhibits sp^3 hybridization about C4′, and a sp^3-hybridized species typically has a strong spectral maximum around 340 nm (*27*); thus, the data suggest that the gem-diamine observed in the X-ray structure of the mutant is not well-populated in solution.

DISCUSSION

A number of studies have demonstrated that essential functional residues in an enzyme are not limited to those residues that are in direct contact with substrates or ligands [e.g., ODC (*13*), trypsin (*28*), dihydrofolate reductase (*29*−*31*), and thymidylate synthetase (*32*−*34*)]. The structural basis for these effects is not well understood but has been postulated to involve conformational changes and alterations in protein dynamics (*32*, *33*). For many enzymes, amino acid residues that form the protein interface between subunits not only function to stabilize the oligomeric structure but also may contribute to the formation of the active site. This is the case for ODC, where the active sites are formed at the subunit interface. A number of residues in the dimer interface of ODC, including Lys-294, contribute long-range interactions that promote efficient catalysis (*13*). Mutation of Lys-294, in particular, increases the K_m for both L-Orn and PLP, reducing the catalytic efficiency of the enzyme. Additional evidence that the mutation affects the active site environment comes from the observation that the spectral properties of PLP in complex with substrate analogues or products are significantly altered. Characterization of the X-ray structure of *T. brucei* K294A ODC confirms that the active site structure has been perturbed by this mutation and suggests that subtle changes in the stability of key regions of the protein may account for the catalytic effects.

The ligands observed bound to the active site in the crystal structure of K294A ODC are highly unusual. All four active sites contain tetrahedral species at C4′ of PLP, with two containing a tetrahedral water, one apparently containing a glycine, and the fourth containing D-Orn, a stereoisomer of the natural substrate L-Orn. Tetrahedral species among Lys-69, PLP, and the ligand have not been previously observed in the ODC active site, as all previous structures (native, D-Orn/G418, putrescine, or DFMO) contained Schiff base species in the active site (*8*, *11*, *12*). The finding that the tetrahedral adducts are stable in the mutant structure suggests that the active site conformation has been altered by the mutation. Importantly, in comparison with the structure of wild-type ODC internal aldimine structure, no conformational change occurs in the position of PLP upon formation of this adduct, suggesting the observed intermediate is a functional species (*8*). The gem-diamine is normally a transient binding intermediate that is not competent for decarboxylation; thus, its greater stability could in part account for the reduced catalytic efficiency of the mutant enzyme. However, on the basis of the spectral analysis, it appears that only a fraction of K294A ODC exists as a gem-diamine species in solution, and we have preferentially crystallized this conformer. A gem-diamine intermediate has previously been observed in a native structure of another PLP-dependent enzyme, L-histidinol phosphate aminotransferase (*35*). In this case, the gem-diamine formation was attributed to the inability of substrate-soaked crystals to undergo productive binding.

The structure reveals several aspects of the mechanism of action and the conformational changes that occur in ODC. Observation of the gem-diamine intermediate of D-Orn on K294A ODC is the first structural evidence of a reaction intermediate that forms along the pathway between the internal and external aldimine species. Comparison of the orientation of D-Orn in the K294A structure with that of Put in the ODC/Put structure demonstrates that a significant rotation must occur for the ligand to reposition from the gem-diamine to the catalytically competent Schiff base structure (Figures 4 and 5). The C4′ (PLP)−αN (D-Orn) bond of the gem-diamine in the K294A ODC structure is perpendicular to the plane of the PLP ring, whereas the C4′ (PLP)−αN (Put) bond of the external aldimine in the ODC/Put structure is parallel to the PLP ring. A rotation of nearly 90° about the C4−C4′ bond of PLP is required to build the extended conjugated system thought to facilitate decarboxylation (*9*). The position of D-Orn in the gem-diamine places αN of D-Orn within 3 Å of a His-197 side chain Nε2. This hydrogen bond is broken as the Schiff base forms, and it is replaced by the hydrogen bond to the C3 hydroxyl of PLP. The proximity of αN of His-197 in the gem-diamine structure suggests that His-197 may be the general acid that abstracts a proton from the gem-diamine intermediate, prior to formation of the external aldimine.

The observed position of D-Orn is very likely to be the initial binding site for the natural substrate L-Orn. Model building suggests that L-Orn would initially bind similarly (relative to PLP) to D-Orn with the C4′ (PLP)−αN (Orn) bond perpendicular to the PLP ring. This binding mode would place both the L- and D-Orn carboxylates on the solvent-exposed side of the ODC active site (away from Lys-69), although with different orientations with respect to PLP. As the C4′−αN bond rotates to form the interaction between αN and the PLP phenolic oxygen moiety, the carboxylate of L-Orn is predicted to swing into the back of the active site pocket toward Lys-69 and Phe-297. Previous mutagenic data demonstrated that Phe-297 is essential for decarboxylation, supporting this orientation for the Schiff base with L-Orn (*36*). The repositioned carboxylate of D-Orn remains on the solvent-exposed active site face and, as observed in the ODC/D-Orn/G418 structure (*12*). In addition, D-Orn does not come into full alignment with the conjugated PLP system of PLP, explaining its poor reactivity as a substrate.

How the mutation of Lys-294 affects the conformational stability of the active site is less clear. The structure of K294A ODC is not different at the site of mutation. Instead, an order−disorder transition occurs in the Lys-169 loop, to which K294 is bound in wild-type ODC, and the extent of this disorder varies for the four monomers in the asymmetric unit. The Lys-169 loop contains Leu-166 which, while disordered in the mutant structure, is positioned within 4.5 Å of D-Orn on the basis of its location in the putrescine-bound structure. On the basis of modeling, this residue is also predicted to form interactions with the carboxylate of L-Orn in the gem-diamine, but not the Schiff base structure. Further, Lys-169 which is also disordered in one active site in the mutant structure forms H-bond interactions with Asp-361, a residue involved in substrate binding (*26*). Thus, we conclude that the main effect of the mutation on activity is mediated by changes in the stability of the Lys-169 loop, which are propagated to the active site loop that contains both Asp-361 and the potential catalytic base, Cys-360 (*11*). Disorder of an active site loop was also observed as a

possible mechanism of allosteric inhibition of ODC by the noncompetitive inhibitor G418 (*24*). Small conformational changes also occur throughout the molecule (<0.5 Å rmsd for the main chain compared with the wild type; Figure 1). These conformational changes correlate somewhat with those observed in comparisons of wild-type ODC to ligand-bound ODCs, suggesting that they are determined by the fold and not by the mutation.

The flexibility in the Lys-169 loop in ODC may be an essential component of the catalytic cycle that is linked to structural changes in the Cys-360 loop. Cys-360 has been observed in two conformations in the available ODC structures, and it is one of the few structural changes that have been correlated with ligand binding (*8*, *11*, *12*). It is typically positioned away from the active site (up position) in unliganded structures and in the inhibited complex with D-Orn (ODC/D-Orn/G418) (*12*), and toward (down position) the active site in structures containing decarboxylated ligands, suggesting these conformational changes are linked to the ODC catalytic cycle (*12*). In the K294A ODC structure, the position of Cys-360 is variable depending on the subunit and it is observed in both the up (active sties A and D) (Cys side chain oriented toward substrate and PLP) and down (active sites B and C) (oriented away) position. The structural data for the K294A ODC mutant suggest that these residues, minimally including Lys-294, Lys-169, and Cys-360, are part of a network of residues organized to undertake concerted motion during the catalytic cycle. Mutation of Lys-294 increases the flexibility of the adjacent Lys-294 and Lys-169 loops, allowing more conformational states to be populated, fewer of which are catalytically competent. In support, an ensemble of conformations are suggested by the finding that the disorder in the Lys-169 loops varies for the four monomers in the asymmetric unit, and by the fact that the four active sites contain different unusual ligand structures and different conformers of Cys-360. Thus, by promoting disorder at the interface, this mutation allows the energy of the reaction coordinate to be dissipated unproductively, unlinking the residues in the pathway that participate in the concerted conformational changes needed for efficient catalysis.

Residues that are energetically coupled to each other in the function of proteins have been identified by the observation of co-evolution of amino acid changes (*37*, *38*). Interestingly, Lys-294 is not an invariant residue in ODC. It is conserved only in those sequences that branch most closely to *T. brucei* ODC by phylogenetic analysis (e.g., mammalian, frog, and *Drosophila* ODCs). However, the position is likely to play the same role in all structures, and sequence changes at position 294 are likely to be paired with conserved changes at other positions in the protein.

The normal function of ODC (and any enzyme) is to channel the substrate−PLP complex through the correct reaction pathway, and ODC is able to bind reaction intermediates and products, thus promoting catalysis. Here we have a glimpse of how very subtle changes in the active site, induced by mutations in a third-shell residue, amino acid Lys-294, can lead to a loss of catalytic efficiency. Lys-294 may be important for stabilizing the ODC active site in a catalytically productive conformation, or it may play a role in concerted dynamic motion required to traverse the complex reaction pathway in an energetically favorable way.

ACKNOWLEDGMENT

We thank Jack Kirsch for useful and stimulating discussions and members of the Goldsmith laboratory, including Xiaoshan Min and Tianjun Zhou, for helpful advice, and Dominika Borek and members of the The University of Texas Southwestern crystallography core facility, specifically Dr. Diana Tomchick and Dr. Mischa Machius, for sharing their structural expertise and for collecting the synchrotron data set. We also thank Andrzej Joachimiak and the staff of the Structural Biology 19-ID beamline. Use of the Advanced Photon Source was supported by the U.S. Department of Energy, Office of Basic Energy Sciences, under Contract W-31-109-Eng-38.

REFERENCES

1. Li, F.-S., Hua, S.-B., Wang, C. C., and Gottesdiener, K. M. (1996) Procyclic *Trypanosoma brucei* cell lines deficient in ornithine decarboxylase activity, *Mol. Biochem. Parasitol. 78*, 227−236.
2. Janne, J., Alhonen, L., and Leinonen, P. (1991) Polyamines: from molecular biology to clinical applications, *Trends Mol. Med. 23*, 241−259.
3. Marton, L., and Pegg, A. (1995) Polyamines as targets for therapeutic intervention, *Annu. Rev. Pharmacol. Toxicol. 35*, 55−91.
4. Wang, C. (1995) Molecular mechanisms and therapeutic approaches to the treatment of African Trypanosomiasis, *Annu. Rev. Pharmacol. Toxicol. 35*, 93−127.
5. Kern, A. D., Olivera, M. A., Coffino, P., and Hackert, M. L. (1999) Structure of mammalian ornithine decarboxylase at 1.6 Å resolution: stereochemical implications of PLP-dependent amino acid decarboxylases, *Structure 7*, 567−581.
6. John, R. A. (1995) Pyridoxal phosphate-dependent enzymes, *Biochim. Biophys. Acta 1248*, 81−86.
7. Grishin, N. V., Phillips, M. A., and Goldsmith, E. J. (1995) Modeling of the spatial structure of eukaryotic ornithine decarboxylases, *Protein Sci. 4* (7), 1291−1304.
8. Grishin, N., Osterman, A., Brooks, H., Phillips, M., and Goldsmith, E. (1999) The X-ray structure of ornithine decarboxylase from *Trypanosoma brucei*: the native structure and the structure in complex with α-difluoromethylornithine, *Biochemistry 38*, 15174−15184.
9. Dunathan, H. C. (1966) Conformation and reaction specificity in pyridoxal phosphate enzymes, *Proc. Natl. Acad. Sci. U.S.A. 55*, 712−716.
10. Brooks, H. B., and Phillips, M. A. (1997) Characterization of the reaction mechanism for *Trypanosoma brucei* ornithine decarboxylase by multiwavelength stopped-flow spectroscopy, *Biochemistry 36* (49), 15147−15155.
11. Jackson, L. K., Brooks, H. B., Osterman, A. L., Goldsmith, E. J., and Phillips, M. A. (2000) Altering the reaction specificity of eukaryotic ornithine decarboxylase, *Biochemistry 39* (37), 11247−11257.
12. Jackson, L. K., Goldsmith, E. J., and Phillips, M. A. (2003) X-ray structure determination of *Trypanosoma brucei* ornithine decarboxylase bound to D-ornithine and to G418, *J. Biol. Chem. 278* (24), 22037−22043.
13. Myers, D. P., Jackson, L. K., Ipe, V. G., Murphy, G. E., and Phillips, M. A. (2001) Long-range interactions in the dimer interface of ornithine decarboxylase are important for enzyme function, *Biochemistry 40* (44), 13230−13236.
14. Osterman, A., Grishin, N. V., Kinch, L. N., and Phillips, M. A. (1994) Formation of functional cross-species heterodimers of ornthine decarboxylase, *Biochemistry 33* (46), 13662−13667.
15. Grishin, N. V., Osterman, A. L., Goldsmith, E. J., and Phillips, M. A. (1996) Crystallization and preliminary X-ray studies of ornithine decarboxylase from *Trypanosoma brucei*, *Proteins 24* (2), 272−273.
16. Otwinoski, Z., and Minor, W. (1997) Processing of X-ray diffraction data collected in oscillation mode, *Methods Enzymol. 276*, 307−326.
17. Navaza, J. (1994) AMoRe: an automated package for molecular replacement, *Acta Crystallogr. A50*, 157−163.
18. Jones, T. A., Zou, J. Y., Cowan, S. W., and Kjeldgaard, M. (1991) *Acta Crystallogr. A47*, 110−119.

19. Brunger, A., Adams, P., Clre, G., Delano, W., Gros, P., Grosse-Kunstleve, R., Jiang, J., Kuszewski, J., Nilges, N., Pannu, N., Read, R., Rice, L., Simonson, T., and Warren, G. (1998) Crystallography and NMR system (CNS): A new software system for macromolecular structure determination, *Acta Crystallogr. D54*, 905−921.
20. Murshudov, G. N., Vagin, A. A., and Dodson, E. J. (1997) Refinement of Macromolecular Structures by the Maximum-Likelihood Method, *Acta Crystallogr. D53*, 240−255.
21. Collaborative Computational Project, No. 4 (1994) The CCP4 suite: programs for protein crystallography, *Acta Crystallogr. D50*, 760−763.
22. Winn, M. D., Isupov, M. N., and Murshudov, G. N. (2001) Use of TLS parameters to model anisotropic displacements in macromolecular refinement, *Acta Crystallogr. 57D*, 122−133.
23. Laskowski, R., MacArthur, M., Moss, D., and Thornton, J. (1993) Procheck: a program to check the stereochemical quality of protein structures, *J. Appl. Crystallogr. 26*, 283−291.
24. Osterman, A., Brooks, H., Rizo, J., and Phillips, M. (1997) The role of Arg-277 in the binding of pyridoxal 5′-phosphate to *Trypanosoma brucei* ornithine decarboxlyase, *Biochemistry 36*, 4558−4567.
25. Sevilla, J. M., Manuel, B., Dominguez, M., and Garcia-Blanco, F. (1992) A study of the Schiff base formed between pyridoxal-5′-phosphate and poly-L-lysine of low polymerization degree, *J. Chem. Soc., Perkin Trans. 2*, 921−926.
26. Osterman, A. L., Kinch, L. N., Grishin, N. V., and Phillips, M. A. (1995) Acidic residues important for substrate binding and cofactor reactivity in eukaryotic ornithine decarboxylase identified by alanine scanning mutagenesis, *J. Biol. Chem. 270* (20), 11797−11802.
27. Morozov, Y. V. (1986) Spectroscopic properties, electronic structure, and photochemical behavior of vitamin B_6 and analogs, in *Vitamin B_6 pyridoxal phosphate: Chemical, biochemical, and medical aspects (Part A)* (Dolphin, D., *et al*., Eds.) pp 131−222, John Wiley & Sons, New York.
28. Hedstrom, L., Sylagi, L., and Rutter, W. (1992) Converting Trypsin to Chymotrypsin: The role of surface loops, *Science 255*, 1249−1253.
29. Rajagopalan, P. T. R., Lutz, S., and Benkovic, S. J. (2002) Coupling interactions of distal residues enhance dihydrofolate reductase catalysis: Mutational effects on hydride transfer rates, *Biochemistry 41*, 12618−12628.
30. Cameron, C. E., and Benkovic, S. J. (1997) Evidence for a functional role of the dynamics of glycine-121 of *Escherichia coli* dihydrofolate reductase obtained from kinetic analysis of a site-directed mutant, *Biochemistry 36*, 15792−15800.
31. Agarwal, P. K., Billeter, S. R., Rajagopalan, P. T. R., Benkovic, S. J., and Hammes-Schiffer, S. (2002) Network of coupled promoting motions in enzyme catalysis, *Proc. Natl. Acad. Sci. U.S.A. 99* (5), 2794−2799.
32. Finer-Moore, J. S., Santi, D. V., and Stroud, R. M. (2003) Lessons and conclusions from dissecting the mechanism of a bisubstrate enzyme: thymidylate synthase mutagenesis, function, and structure, *Biochemistry 42*, 248−256.
33. Birdsall, D. L., Finer-Moore, J. S., and Stroud, R. M. (2003) The only active mutant of thymidylate synthase D169, a residue far from the site of methyl transfer, demonstrates the exquisite nature of enzyme specificity, *Protein Eng. 16* (3), 229−240.
34. Kawate, H., Landis, D. M., and Loeb, L. A. (2002) Distribution of mutations in human thymidylate synthase yielding resistance to 5-fluorodeoxyuridine, *J. Biol. Chem. 277* (39), 36304−36311.
35. Sivaraman, J., Li, Y., Larocque, R., Schrag, J. D., Cygler, M., and Matte, A. (2001) Crystal structure of histidinol phosphate aminotransferase (HisC) from *Escherichia coli*, and its covalent complex with pyridoxal-5′-phosphate and L-histidinol phosphate, *J. Mol. Biol. 311*, 761−776.
36. Jackson, L., Brooks, H., Myers, D., and Phillips, M. (2003) Ornithine decarboxylase promotes catalysis by binding the carboxylate in a buried pocket containing phenylalanine 397, *Biochemistry 42* (10), 2933−2940.
37. Lockless, S. W., and Ranganathan, R. (1999) Evolutionarily conserved pathways of energetic connectivity in protein families, *Science 286* (8), 295−299.
38. Suel, G. M., Lockless, S. W., Wall, M. A., and Ranganathan, R. (2003) Evolutionarily conserved networks of residues mediate allosteric communication in proteins, *Nat. Struct. Biol. 10* (1), 59−69.
39. Kraulis, P. (1991) MOLSCRIPT: a program to produce both detailed and schematic plots of protein structures, *J. Appl. Crystallogr. 24*, 946−950.
40. Esnousf, R. M. (1997) An extensively modified version of Molscript that includes greatly enhanced coloring capabilities, *J. Mol. Graphics 15*, 132−134.
41. Murshudov, G., Vagin, A., and Dodson, E. (1997) Refinement of Macromolecular Structures by the Maximum-Likelihood Method, *Acta Crystallogr. D53*, 240−255.
42. Esnousf, R. M. (1999) Further additions to Molscript version 1.4, including reading and contouring of electron density maps, *Acta Crystallogr. D55*, 938−940.

BI048933L